ELSEVIER

Earth and Planetary Science Letters 180 (2000) 415–423

EPSL

www.elsevier.com/locate/epsl

SiO_2 precipitation in olivine: ATEM investigation of two dunites annealed at 300 MPa in hydrous conditions

Paul Raterron [a,1,*], Prame Chopra [b], Jean-Claude Doukhan [a]

[a] *Laboratoire Structure et Propriétés de L'État Solide (associated to CNRS), Université Sciences et Technologies de Lille, 59655 Villeneuve d'Ascq Cedex, France*

[b] *Department of Geology, Australian National University, Canberra, A.C.T. 0200, Australia*

Received 5 August 1999; accepted 24 May 2000

Abstract

Two natural dunites were annealed at pressure $P = 300$ MPa, temperature $T = 1373$, 1473 and 1573 K, and fO_2 within the stability field of olivine. The starting materials contained small amounts of hydroxyls in the form of minor phases of hydrated minerals, which released an aqueous phase during the experiments. A detailed analytical transmission electron microscopy (ATEM) investigation of these materials revealed that small quantities of two types of silica-rich glass formed during heat treatment. The first type of glass, found at triple junctions as rare partially crystallized glass pockets, results from melting dehydration reactions involving the hydrous phases. The second type of glass is found as pure silica precipitates (0.1–0.5 μm in size, for a total of a few 0.1 vol%) within the olivine grains of specimens heated to ≥1473 K. From considerations of the kinetics of the precipitation at 1473 K, we interpret this silica precipitation as resulting from the condensation of olivine metallic vacancies promoted by increasing fluid fugacities during the runs. Our observations, thus, demonstrate that metastable silica can precipitate in olivine from dunites experiencing rapid changes in their thermodynamical environment.

Keywords: olivine; dunite; transmission electron microscopy; silica; precipitation; exsolution; point defects; ultramafic composition; xenoliths

1. Introduction

Mantle-derived peridotite xenoliths often contain glasses along grain boundaries, triple junction and/or in large inclusions (> 100 μm) within minerals. In many cases these glasses exhibit a distinctive chemistry (e.g. [1–3], and references therein) characterized by relatively high concentrations of silica (up to 75 wt%). The unusual chemistry and wide geographic and tectonic provenance of these melts has led to a vigorous debate on their origins (e.g. [4–6]). Also, experimental annealing of diopside and enstatite single crystals and/or peridotitic material produces silica-rich precipitates (so-called early partial melting (EPM) precipitates) in pyroxenes at sub-solidus temperatures (e.g. [7–10]). Sili-

* Corresponding author. Tel.: +1-631-632-6853; Fax: +1-516-632-8140; E-mail: paul.raterron@univ-lille1.fr, raterron@sbmp04.ess.sunysb.edu

[1] Present address: Center for High Pressure Research and Mineral Physics Institute, Department of Geosciences, ESS Building, SUNY at Stony Brook, Stony Brook, NY 11794-2100, USA.

0012-821X/00/$ – see front matter
PII: S0012-821X(00)00160-6

ca precipitation has also been observed in olivine grains of a lherzolite experimentally annealed above its solidus in hydrous conditions ([10]). Whether this silica precipitation observed in ultramafic materials is of importance for the understanding of natural silica-rich melts in xenoliths or is an experimental 'artifact' has been unclear.

In the present study we have investigated the development of such a silica-rich precipitation in two spinel-bearing dunites annealed at sub-solidus temperatures in the laboratory. Their experimental treatment, involving rapid changes in the pressure and temperature conditions and important changes in the O_2 and H_2O and/or H_2 fugacities, was in many aspects similar to that experienced by xenoliths during their entrainment and subsequent emplacement in the crust. The aim of this study was thus to characterize by analytical transmission electron microscopy (ATEM) the morphology, composition and kinetics of the SiO_2-rich precipitation in two olivine assemblages experiencing rapid thermodynamical changes.

2. Starting material, annealing conditions, and ATEM procedure

Two natural dunites were experimentally annealed in a Paterson machine [11] at temperatures between 1373 and 1573 K, in the presence of water. The starting dunites were chosen because (1) they are natural olivine assemblages containing small amounts of orthopyroxene (OPX) that buffer the activity of silica (a_{SiO_2}), (2) as with many dunites they chemically equilibrated in nature in a range of pressure accessible to a Paterson machine, and (3) they contain trace quantities of the hydrous minerals, due to minor metasomatism that dehydrate and release H_2O under the experimental P,T conditions. IR measurements carried out on the same dunites after similar experiments [12] revealed that water is still present in the assembly at the end of the runs, and thus that the samples remain under hydrous conditions throughout the annealing. The investigated dunites were also deformed because, as previously observed in pyroxenes (e.g., [7]) the silica-rich precipitates tend to nucleate preferentially on dislocation cores. Detailed petrographic descriptions of both starting materials are given in [13] and [14]. The modal composition of the starting Aheim dunite is 96% olivine, 2% pyroxenes, 2% hydrous layer silicate minerals (mainly clinochlore and phlogopite) and $<1\%$ spinel. This rock has a unimodal olivine grain size distribution with an average size of about 900 μm. The Anita Bay dunite consists of 94% olivine, 5% pyroxenes and 1% chromite together with a widespread but minor occurrence along grain boundaries of hydrous secondary minerals (mainly clinochlore, tremolite and talc). Specimens from the Anita Bay dunite were cored in a region with an average grain size of about 100 μm.

Three specimens were cored in each of the starting dunites. The annealing conditions are given in Table 1. Experiments proceeded by first raising the confining pressure to $\sim$200 MPa and then increasing the temperature at a typical rate of $\sim 0.3\ K_s^{-1}$ until the intended temperature was reached and the pressure had risen to 300 MPa.

Table 1
Annealing conditions at 300 MPa

Sample	Specimen material: dunite	Soak temperature (K)	Duration at soak temperature (s)	Silica precipitates detected
4439[a]	Aheim	1373	13860	no
4436[b]	Aheim	1473	720	yes
4468	Aheim	1573	1680	yes
4271[b]	Anita Bay	1368	85920	no
4569	Anita Bay	1473	12060	yes
4497	Anita Bay	1573	780	yes

[a]results of [14]
[b]results of [13]

Samples were cooled at a rate of $\sim 1.3\ K_s^{-1}$. Specimens were annealed in the presence of the water released by the hydrous minerals. Chlorite transforms into enstatite, $MgAl_2O_4$ spinel and forsterite, and releases H_2O above $T = 1073$ K and $P > 300$ MPa (e.g., [15]). Talc similarly transforms into enstatite and cristobalite (which in contact with olivine forms enstatite) and releases H_2O under equivalent P/T conditions. At high temperature the specimens, thus, consisted mainly of olivine crystals in the presence of an aqueous phase with small amounts of enstatite and spinel.

All specimens, except for 4271, were enclosed in a long Fe sealing jacket. The latter specimen was enclosed in a short Ni jacket (ibid.). The main role of these metallic jackets was to prevent the gas confining medium entering the specimen. The use of Fe capsule directly in contact with olivine is also recommended to maintain the olivine in its redox stability field (see [16], and references therein). In the case of our samples, the presence in the assembly of small amounts of H_2O (released from hydrous minerals) renders the system more complex and does not allow a precise estimate of the oxygen fugacity (fO_2). The absence of Fe-precipitates in the olivine grains at the end of the run, and the clear light green color of the recovered material, suggest however that the olivine remained within its redox stability field during the runs.

Specimens for ATEM were cut in optically selected areas of doubly polished standard petrographic sections. They were ion-thinned to electron transparency (argon beam accelerated at 5 kV) and coated with a carbon layer. A Philips CM30 electron microscope, operating at 300 kV and equipped with an energy dispersive X-ray (EDX) spectrometer (Noran-Voyager), was used to investigate the specimens. This EDX spectrometer has a germanium detector and an ultra-thin window, which allows the detection and quantification of oxygen. We calibrated the so-called Cliff and Lorimer K-factors by the [17] method, with silicate and silicide standards. Microanalyses were mostly performed in the STEM mode on scanned areas (≥ 100 nm^2) to prevent the lost of elements during the microanalysis (particularly critical when analyzing silicate glasses). Despite this procedure, we could not always prevent the loss of alkali (particularly of Na). We used the [18] meth-

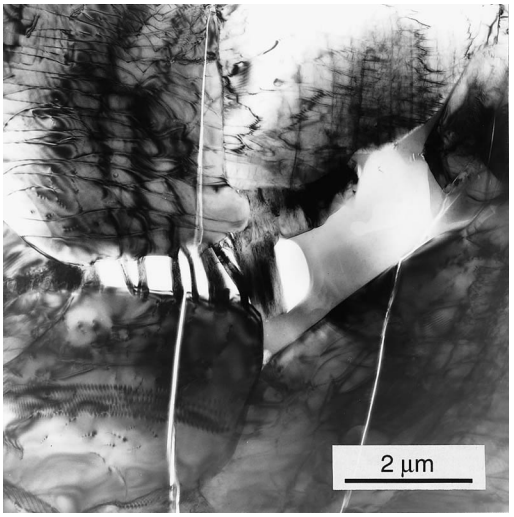

Fig. 1. TEM micrograph (bright field) of a glass pocket at a triple junction (sample #4497). Note that part of the pocket is recrystallized. This glass results from reactions involving hydrous minerals.

Table 2
Olivine compositions (wt%) and Mg/(Mg+Fe) ratio (at%) after the experiments

Average	2	6	8	2	3	6
Sample	4439	4436	4468	4271	4569	4497
SiO_2	41.3	41.3	41.4	41.2	41.5	41.2
FeO	7.56	7.20	7.10	7.74	8.53	7.74
MnO	0.08	0.11	0.11	0.10	0.15	0.09
MgO	50.8	50.9	51.0	50.5	49.3	50.6
NiO	0.38	0.42	0.38	0.40	0.43	0.40
Mg/(Mg+Fe)	92.3(0.5)	92.6(0.5)	92.8(0.2)	92.1(0.4)	91.3(1.1)	92.1(0.4)

Note: numbers in parentheses are the larger of the statistical (two standard deviations) and dispersion uncertainties.

Table 3
Enstatite compositions (wt%) and Mg/(Mg+Fe) ratio (at%) after the experiments

Average	1	2	4	2	1	3
Sample	4439	4436	4468	4271	4569	4497
SiO_2	58.4	58.5	58.9	58.3	58.5	58.1
TiO_2	–	–	0.02	–	–	–
Al_2O_3	0.18	0.30	0.01	0.15	–	0.30
FeO	5.27	4.18	4.33	5.51	5.17	5.44
MnO	0.10	0.07	0.12	0.12	0.21	0.13
MgO	35.8	36.7	36.5	35.7	35.8	35.7
CaO	0.11	0.04	–	0.05	0.08	0.10
Cr_2O_3	0.04	–	0.02	0.07	0.11	0.08
NiO	0.11	0.16	0.06	0.11	0.11	0.07
Mg/(Mg+Fe)	92.4(0.4)	93.9(0.6)	93.7(1.1)	92.1(0.5)	92.5(0.5)	92.1(0.5)

Note: numbers in parentheses are the larger of the statistical (two standard deviations) and the dispersion uncertainties.

od for the thickness correction (more details in [19]). To compute the cation site occupancies we assumed that iron only occurs as Fe^{2+} and that the H concentration was negligible.

3. ATEM observations and interpretation

In all the investigated specimens, we observed rare pockets of glass at triple junctions and/or phase boundaries (Fig. 1). These pockets have in some cases partially crystallized and exhibit systematically large SiO_2 and Al_2O_3 contents (55–80 and 12–20 wt%, respectively). They also contain relatively high concentrations of K_2O (typically 2–4 wt% K_2O) and trace amounts of Cl. We interpret these glass pockets as resulting from reactions involving the hydrous minerals present in the starting materials. Such reactions which have previously been inferred in experimentally annealed Anita Bay dunite samples ([20]), must have released water during the runs.

In both the Aheim and Anita Bay samples, the olivine and pyroxenes grains exhibit microstruc-

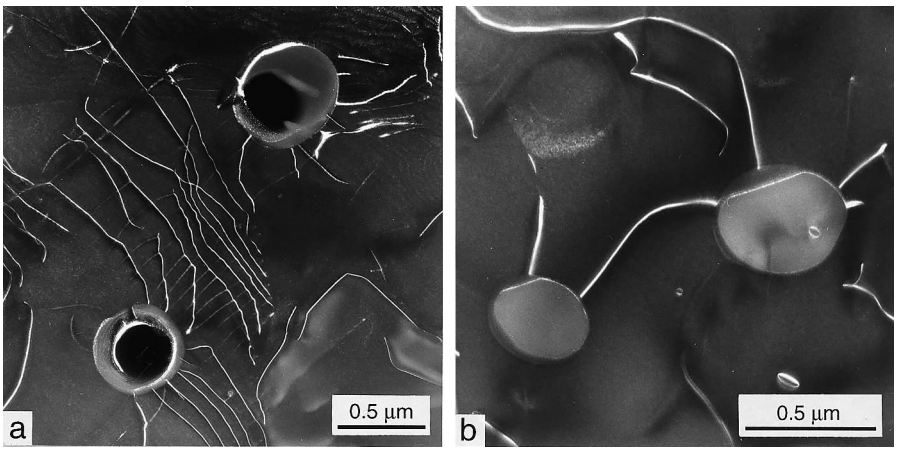

Fig. 2. Dark field TEM micrographs of intracrystalline glass droplets in olivine (sample #4468) (a) Two droplets interacting with a subgrain boundary. They exhibit the shape typical of EPM droplets (an ellipsoidal glassy phase with a central hole). Carbon stains left by the microanalysis are visible on the top of one of the droplets. (b) EPM droplets in a thin area. The droplet on the right hand side of the figure corresponds to analysis #25bis (Table 4). The presence of a small dislocation loop shows that a thin layer of olivine was present in the analyzed column (see text).z

tures typical of high temperature deformation. We detect in olivine a rather homogeneous density of free dislocations (10^{13} m^{-2} in samples deformed at 1573 K) with both **a** and **c** Burgers vectors. The enstatite crystals contain numerous thin lamellae of clino-enstatite, which probably result from stress-induced ortho- to clino-enstatite inversion during cooling. These lamellae overprint any other defect features, such as dislocations or precipitates, which thus were not characterized in enstatite. The compositions of olivine and enstatite averaged over several analyses in each specimen are reported in Tables 2 and 3. These compositions are practically identical to the olivine and enstatite compositions in the starting materials.

In the four samples annealed at $T \geq 1473$ K we also detected numerous tiny rounded glass precipitates within the olivine grains (Fig. 2), often interacting with dislocations and sub-grain boundaries. These precipitates are very small (typically 0.5 μm in diameter) and sparsely distributed in the olivine matrix, representing roughly less than a few 0.1 vol% of the investigated material. No reaction rim between these glasses and the surrounding host olivine were detected. Microanalyses of these tiny glass bodies raised a technical problem: because of their small size, the measured raw compositions, sorted by increasing SiO_2 contents in Table 4, correspond to mixtures of glass and olivine. We measure up to 95.3 wt% SiO_2 (analysis 25bis) for the object shown on the right hand side of Fig. 2b, which still corresponds to a mixture of glass and olivine as revealed by the dislocation loop overlying it. The varying amounts of olivine 'contamination' in the analyses of Table 4 are highlighted in Fig. 3. Both MgO and NiO concentrations when plotted against SiO_2 fall on straight lines between the composition of the olivine and pure SiO_2. The same conclusion can be drawn from the mineral norms (Table 4) consistent with a mineralogical association of quartz and olivine (with trace amounts of corundum). Finally, the data in Table 4 exhibit the same Mg/(Mg+Fe) ratio as the olivine. This suggests that the detected Mg and Fe are hosted only in the olivine matrix. Thus all of the analyses in Table 4 are explicable in terms of a simple mixing of olivine and SiO_2.

4. Discussion

Of the two types of glass that have been identified in the annealed samples, the glass pockets found at triple junctions and/or phase boundaries have been derived from melting associated with dehydration of trace hydrous minerals initially present in both dunites. Given this mode of formation (dehydration reactions of alteration material) and the observations of crystallization features (Fig. 1), the chemistry of these glass pockets will therefore not be discussed further.

The other type of glass, consisting of SiO_2 precipitates in the olivine matrix, is of importance for

Table 4
Raw droplet/olivine-matrix compositions (wt%) and computed norms for sample 4468

Analysis	26	25	24	27	25bis
SiO_2	44.3	62.5	77.0	84.4	95.3
Al_2O_3	0.21	–	0.48	0.13	–
FeO	4.31	4.42	1.53	0.91	0.54
MnO	–	0.10	–	0.05	0.07
MgO	50.9	32.7	20.5	14.3	4.05
NiO	0.30	0.22	0.16	0.05	0.04
Total	100.02	99.94	99.67	99.84	100.00
Mg/(Mg+Fe)	92.2(0.4)	93.0(0.4)	93.0(1.4)	94.0(0.7)	93.1(1.4)
quartz	4.4	36.1	61.2	73.4	92.0
corundum	0.2	–	0.5	0.1	–
fayalite	6.6	6.8	2.4	1.5	1.0
forsterite	88.8	57.1	35.9	25.0	7.0

Note: numbers in parentheses are 2σ standard deviations.

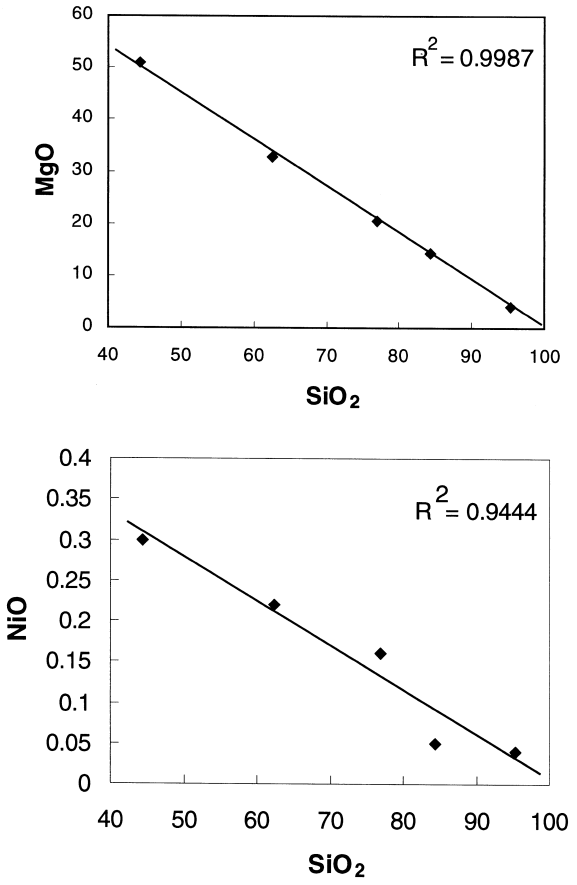

Fig. 3. Relationships between SiO_2 and the MgO and NiO contents (in wt%) of the raw compositions of the glass inclusions observed in olivine (Table 4). These compositions are explicable in terms of simple two-phase mixing involving the phases olivine and pure SiO_2.

the understanding of olivine chemistry. The following discussion is thus focussed on the interpretation of this silica precipitation. As a background for this discussion, we use a thermodynamical model proposed for the olivine point defect chemistry by [21] (noted N and S in the following) in their now classic article. In the framework of this model, the majority point defects in olivine are the Fe^{3+} cations in either octahedral (Me) or tetrahedral (Si) sites, as well as the octahedral vacancies (see also [22]). We chose this model because it allows a full description of the olivine solid–solution $(Fe_xMg_{1-x})_2SiO_4$ within its stability field. Also, the Me vacancies have been observed by thermogravimetric measurements in both fayalite and olivine (e.g. [21], and references therein), and ferric iron on Si site has been observed in forsterite using electron paramagnetic resonance [23]. Finally, the N and S's model has been verified several times by independent studies of reactions and/or equilibria involving olivine (e.g., [24,16]).

4.1. The SiO_2/olivine equilibrium

According to [21] (their equation 3), the SiO_2/olivine equilibrium, in the presence of oxygen, can be described by the following equation (in olivine $Fo_{100-\delta}$, Fe_2SiO_4 has the dilution δ%):

$$Fe_2SiO_4 + 2\,V''_{Me} + 4\,Fe^{\bullet}_{Me} = SiO_2 + O_2(g) + 6\,Fe^{X}_{Me} \quad (1)$$

where V''_{Me}, $Fe^{\bullet}_{Me}$, and Fe^{X}_{Me} are respectively divalent Me vacancies, Fe^{3+} cations, and Fe^{2+} cations, in Me sites, using the standard Kröger and Vink's notation for point defects (see [25]). Eq. 1 does not allow a full description of the thermodynamical state of olivine in contact with oxygen and silica. At constant T and P, two other equations are needed, e.g. the electroneutrality condition (linking the charges of the defects) and the equation describing the equilibrium between olivine and oxygen (see [21]). Eq. 1, however, shows that the exsolution of SiO_2 from the olivine solid–solution does not actually require silicon diffusion. It also shows that exsolution of SiO_2 tends to reduce the concentrations of both V''_{Me} and $Fe^{\bullet}_{Me}$ defects, and thus to move the olivine toward a stoichiometric composition. In a context of a dynamical equilibrium, this tendency could be compensated continually by, for example, the incorporation of oxygen (due for instance to an increasing fO_2) which, conversely, would tend to increase both the V''_{Me} and the $Fe^{\bullet}_{Me}$ concentrations (e.g. [21] equation 19).

N and S's model does not account for the 'water' point defects, e.g. interstitial H^+ or OH^- substituted for O^{2-}, likely to be present in our assemblages annealed under hydrous conditions.

According to a number of authors (e.g. [26–28]) 'water' defects substitute for ferric iron in the olivine solid–solution. Hence, an increasing 'water' defect concentration, due for instance to increasing H_2O and/or H_2 fugacities (fH_2O and fH_2, respectively) would tend to increase the V''_{Me} concentration, and thus to promote more precipitation of SiO_2 (see Eq. 1). Fluid fugacities, fO_2, fH_2O and fH_2, may therefore play very similar roles with respect to the exsolution of silica. Such an exsolution can actually occur over wide ranges of fO_2. [24] calculated that, at 1 atm. and 1573 K, SiO_2 can precipitate in Fo_{90} for $10^{-14} < fO_2 < 10^{-5.4}$ MPa (fO_2 is here assimilated to pO_2). The SiO_2 precipitation is however limited in quantity since it ultimately depends on the concentration of V''_{Me} in the olivine solid–solution. This concentration has been estimated to be on the order of 0.1% per site (i.e. 0.2% per mol) in the San Carlos olivine (Fo_{90}), which equilibrated in nature under relatively high fO_2, as did the olivine crystals used in the present study.

Silica precipitation in olivine is then quite understandable in the framework of N and S's model by considering the equilibria involving olivine and several fluids such as O_2 and/or H_2O, and eventually the silica phase. In the case of our assemblages, containing primary enstatite and spinel grains, such silica precipitation cannot correspond to equilibrium since, given the run temperatures, silica should eventually react with the surrounding Fo_{92} to form enstatite (see [29]). The presence of pure silica precipitates in the olivine grains, thus, strongly suggests that equilibrium was not achieved at the end of the runs. In order to interpret the observed metastable SiO_2, one must therefore take into consideration the kinetic aspects of the silica precipitation.

4.2. Kinetics of SiO_2 precipitation in olivine

We observed that SiO_2 precipitates were readily produced in experiment 4436 which had a peak temperature of 1473 K and a soak duration of only 12 min. Such rapid kinetics suggests that the SiO_2 exsolution is controlled by species having high intracrystalline diffusivities at 1473 K, i.e. able to diffuse over long distances (reasonable fractions of the grain size) during the runs. The only species that fulfill this requirement, in the framework of the model described above, are the Me vacancies V''_{Me} and the potential 'water' defects, all defects associated with the ferric/ferrous iron transition for charge compensation. Indeed, the Fe–Mg interdiffusion coefficient in olivine is about $D_{Fe/Mg} = 10^{-11}$ cm^2/s at 1473 K [30,31]. This roughly corresponds to a V''_{Me} diffusion coefficient of $D_{V_{Me}} \geq 10^{-8}$ cm^2/s, since V''_{Me} concentration per site ($[V''_{Me}]$) should not exceed 0.1% in olivine at this temperature (V''_{Me} diffusion coefficient can be estimated by dividing $D_{Fe/Mg}$ by $[V''_{Me}]$). In other words, Me vacancies are able to migrate over distances ≥ 50 μm during a 12-min long annealing at 1473 K. 'Water' defects have an even higher mobility in olivine, and are able to diffuse over distances ≥ 2 mm in 12 min at 1473 K (see [26]). Unlike V''_{Me} and 'water' defects, the Mg and Fe cations can only diffuse over short distances (typically < 2 μm) during a 12-min run at 1473 K, while silicon and oxygen can almost be considered immobile under the same conditions, because $D_{Si} = 10^{-17}$ cm^2/s at 1473 K, and D_O is about two orders of magnitude higher than D_{Si} (e.g. [32,33]).

In summary, our observations suggest that the kinetics of silica precipitation in olivine is controlled by the diffusion of V''_{Me} defects and possibly 'water' defects. During this process, the Mg and Fe cations may have moved a few micrometers away from the transformed area (consisting now of silica), while Si and O were readily immobile. We thus interpret the silica precipitation as a vacancy (V''_{Me}) condensation process, induced by an increase in the V''_{Me} and/or 'water' defect concentrations during the runs (see Eq. 1); such an increase would be the result of increasing fluid fugacities due to the dehydration reactions occurring at triple junctions. A similar explanation (metallic vacancy condensation) is proposed by [9] to explain the experimentally induced precipitation of silica in diopside.

This interpretation also explains why, in our experiment, the exsolved silica did not react with the adjacent olivine to form enstatite. Because of the different diffusivities of the considered species, the olivine grains were able to reach the equilib-

rium in terms of fO_2, fH_2O and/or fH_2 (V''_{Me} and/or 'water' defects diffusion, and $Fe^{2+/3+}$ transition), but not in terms of the activity of silica. Full equilibration of the olivine, as well as the silica precipitates, with the rest of the assembly may require time duration allowing the diffusion of every species, including the Fe, Mg and Si cations, throughout the olivine grains. Using the D_{Si} value given above, it would thus take about 2 years at 1473 K to fully equilibrate a 100-μm grain size assemblage (average diffusion distance: 50 μm). Even if this equilibration process is probably enhanced by chemical driving forces and the presence of dislocations in the crystals (diffusion short cuts), it is likely to have a slow kinetics when compared to short geological events, such as the ascent of xenolithic materials during volcanic eruptions.

5. Conclusion

Exsolution of pure SiO_2 in olivine is consistent with the now classic model proposed by [21] for the olivine solid–solution. Silica precipitates, however, are likely to have only a transient existence in ultramafic assemblages such as the studied dunites, and to eventually re-equilibrate with the surrounding material, for example by reacting with the adjacent olivine to form enstatite. This equilibration process, however, is likely to involve the intracrystalline diffusion of slow species (such as Si cations) throughout the olivine grains, and thus to have a slow kinetics. Because of this slow kinetics, silica precipitates may also form and be preserved within the olivine grain from xenoliths that experienced rapid thermodynamical changes during their ascent to the surface. Indeed, silica-rich precipitates have already been observed in as-found pyroxenes from xenoliths ([8]). Further TEM investigation of xenolithic material is thus required to check for silica precipitates in olivine. Further investigations are also required to find out whether such metastable silica precipitation could contribute to some extent to the silica-rich melts observed in ultramafic xenoliths worldwide.

Acknowledgements

This is Publication number 216 from the National Key Centre for the Geological Evolution and Metallogeny of Continents. The ATEM work was supported by the CNRS-INSU (programme DBT). The authors thank S. Mackwell, P. Schiano and M. Seyler, for helpful discussions and critical reading of early drafts. This article also benefited from the constructive reviews of R. Cooper and an anonymous reviewer.*[EB]*

References

[1] P. Schiano, R. Clocchiatti, Worldwide occurrence of silica-rich melts in sub-continental and sub-oceanic mantle minerals, Nature 368 (1994) 621–623.
[2] R. Wirth, Thin amorphous films (1–2 nm) at olivine grain boundaries in mantle xenoliths from San Carlos, Arizona, Contrib. Mineral. Petrol. 124 (1996) 44–54.
[3] G.M. Yaxley, V. Kamenetsky, D.H. Gren, T.J. Falloon, Glasses in mantle xenoliths from western Victoria, Australia, and their relevance to mantle processes, Earth. Planet. Sci. Lett. 148 (1997) 433–446.
[4] M.B. Baker, M.M. Hirschmann, M.S. Ghiorso, E.M. Stolper, Compositions of the near-solidus peridotite melts from experiments and thermodynamic calculations, Nature 375 (1995) 308–311.
[5] T.J. Falloon, D.H. Green, H.St.C. O'Neill, W.O. Hibberson, Experimental tests of low degree peridotite partial melt compositions: implications for the nature of anhydrous near-solidus peridotite melts at 1 GPa, Earth Planet. Sci. Lett. 152 (1997) 149–162.
[6] P. Schiano, B. Bourdon, On the preservation of mantle information in ultramafic nodules: glass inclusions within minerals versus interstitial glasses. Earth Planet. Sci. Lett., 1999, in press.
[7] J. Ingrin, N. Doukhan, J.C. Doukhan, High-temperature deformation of diopside single crystal, 2, TEM investigation of the induced defect microstructures, J. Geophys. Res. 96 (1991) 14287–14297.
[8] N. Doukhan, J.C. Doukhan, J. Ingrin, O. Jaoul, P. Raterron, Early partial melting in pyroxenes, Am. Mineral. 78 (1993) 1247–1257.
[9] O. Jaoul, P. Raterron, High-temperature deformation of diopside crystal, 3, Influences of pO_2 and SiO_2 precipitation, J. Geophys. Res. 99 (1994) 9423–9439.
[10] P. Raterron, G.Y. Bussod, N. Doukhan, J.C. Doukhan, Early partial melting in the upper mantle: an A.E.M. study of a lherzolite experimentally annealed at hyperolidus conditions, Tectonophysics 279 (1997) 79–91.
[11] M.S. Paterson, A high pressure, high temperature appa-

ratus for rock deformation, Int. J. Rock Mech. Miner. Sci. 7 (1970) 517–526.
[12] P.N. Chopra, M.S. Paterson, The role of water in the deformation of dunite, J. Geophys. Res. 89 (1984) 7861–7876.
[13] P.N. Chopra, M.S. Paterson, The experimental deformation of dunite, Tectonophysics 78 (1981) 453–473.
[14] P.N. Chopra, High-temperature transient creep in olivine rocks, Tectonophysics 279 (1997) 93–111.
[15] D.M. Jenkins, J.V. Chernosky Jr., Phase equilibria and crystallochemical properties of Mg-Chlorite, Am. Mineral. 71 (1986) 924–936.
[16] P. Raterron, F. Béjina, R.C. Liebermann, O. Jaoul, J.C. Doukhan, Olivine/Fe-metal equilibrium under high pressure: ATEM investigation of chemical exchanges between experimentally annealed samples and Fe capsules, Phys. Chem. Miner. 25 (1998) 485–493.
[17] E. Van Cappellen, The parameterless correction method in X-ray microanalysis, Microsc. Microanal. Microstruct. 1 (1990) 1–22.
[18] E. Van Cappellen, J.C. Doukhan, Quantitative transmission X-ray microanalysis of ionic compounds, Ultramicroscopy 53 (1994) 343–349.
[19] P. Raterron, M.A. Carpenter, J.C. Doukhan, Sillimanite mullitization: ATEM investigation and point defect model, Phase Transit. 68 (1999) 451–500.
[20] N. Doukhan, J.C. Doukhan, J.D. Fitz Gerald, P.N. Chopra, M.S. Paterson, A TEM microstructural study of experimentally deformed Anita bay Dunite, in: R.E. Tressier, R.C. Bradt (Eds.), Deformation of Ceramics II, Plenum Press, New York, 306 pp, 1984.
[21] A. Nakamura, H. Schmalzried, On the nonstoichiometry and point defects of olivine, Phys. Chem. Miner. 10 (1983) 27–37.
[22] M. Hillert, M. Selleby, B. Sundman, A reassessment of the non-stoichiometry of fayalite, Phys. Chem. Miner. 23 (1996) 387–390.
[23] H. Rager, S. Hosoya, G. Weiser, Electron paramagnetic resonance and polarized optical absortion spectra of Ni^{2+} in synthetic forsterite, Phys. Chem. Miner. 15 (1988) 383–389.
[24] O. Jaoul, B. Houlier, M. Cheraghmakani, R. Pichon, R.C. Liebermann, Surface destabilization and laboratory-induced non-stoichiometry in San Carlos olivine, Phys. Chem. Miner. 15 (1987) 41–53.
[25] F.A. Kröger, 1974. The chemistry of imperfect crystal, 2nd edn., 1039 pp., North-Holland, New York.
[26] S.J. Mackwell, D.L. Kohlstedt, Diffusion of hydrogen in olivine: implication for water in the mantle, J. Geophys. Res. 95 (1990) 5079–5088.
[27] Q. Bai, D.L. Kohlstedt, Substitutional hydrogen solubility in olivine and implications for water storage in the mantle, Nature 357 (1992) 672–674.
[28] K. Wright, C.R.A. Catlow, A computer simulation study of (OH) defects in olivine, Phys. Chem. Miner. 20 (1994) 515–518.
[29] U. Nitsan, Stability field of olivine with respect to oxidation and reduction, J. Geophys. Res. 79 (1974) 705–711.
[30] D.K. Buening, P.R. Buseck, Fe–Mg lattice diffusion in olivine, J. Geophys. Res. 78 (1973) 6852–6862.
[31] O. Jaoul, Y. Bertran-Alvarez, R.C. Liebermann, D.G. Price, Fe–Mg interdiffusion in olivine up to 9 GPa at $T = 600$–$900°C$; experimental data and comparison with defects calculations, Phys. Earth Planet. Int. 89 (1995) 199–218.
[32] B. Houlier, O. Jaoul, F. Abel, R.C. Liebermann, Oxygen and silicon self-diffusion in natural olivine at $T = 1300°C$, Phys. Earth Planet. Int. 50 (1988) 240–250.
[33] F. Béjina, O. Jaoul, Silicon diffusion in silicate minerals, Earth Planet. Sci. Lett. 153 (1997) 229–238.